FEBS Letters

FEBS PR
science publishing b

Crystal structure of peptide-bound neprilysin reveals key binding interactions

Journal:	*FEBS Letters*
Manuscript ID	FEBSL-19-0870.R2
Wiley - Manuscript type:	Research Articles
Date Submitted by the Author:	n/a
Complete List of Authors:	Moss, Stephen; University of Bath, Biology and Biochemistry Subramanian, Vasanta; University of Bath, Biology and Biochemistry Acharya, K. Ravi; University of Bath, Biology and Biochemistry
Keywords:	Neprilysin, Protein structure, Crystallography, Neutral endopeptidase, Substrate-bound, Peptide bound, Zinc metalloprotease
Abstract:	Neprilysin (NEP) is a promiscuous zinc metalloprotease with a broad substrate specificity and cleaves a remarkable diversity of substrates through endopeptidase action. Two of these - amyloid-β and natriuretic peptides - implicate the enzyme in both Alzheimer's disease and cardiovascular disease respectively. Here, we report creation of a catalytically inactive NEP (E584D) to determine the first peptide-bound crystal structure at 2.6 Å resolution. The structure reveals key interactions involved in substrate binding which we have identified to be conserved in other known zinc metalloproteases. In addition, the structure provides evidence for a potential exosite within the central cavity that may play a critical role in substrate positioning. Together, these results contribute to our understanding of the molecular function of NEP.

Crystal structure of peptide-bound neprilysin reveals key binding interactions

Stephen Moss, Vasanta Subramanian, K. Ravi Acharya*

Department of Biology and Biochemistry, Claverton Down, University of Bath, Bath BA2 7AY, UK

*Corresponding author at: Department of Biology and Biochemistry, University of Bath, Claverton Down, Bath BA2 7AY, UK.

E-mail: bsskra@bath.ac.uk (K. Ravi Acharya)

Abstract

Neprilysin (NEP) is a promiscuous zinc metalloprotease with a broad substrate specificity and cleaves a remarkable diversity of substrates through endopeptidase action. Two of these - amyloid-β and natriuretic peptides - implicate the enzyme in both Alzheimer's disease and cardiovascular disease respectively. Here, we report creation of a catalytically inactive NEP (E584D) to determine the first peptide-bound crystal structure at 2.6 Å resolution. The structure reveals key interactions involved in substrate binding which we have identified to be conserved in other known zinc metalloproteases. In addition, the structure provides evidence for a potential exosite within the central cavity that may play a critical role in substrate positioning. Together, these results contribute to our understanding of the molecular function of NEP.

Keywords: Neprilysin, NEP, Neutral endopeptidase, Zinc metalloprotease, Protein structure, Crystallography, Peptide-bound.

Abbreviations: NEP, Neprilysin; CNP, C-type natriuretic peptide; PEG, polyethylene glycol; IDE, Insulin-degrading enzyme; ECE-1, Endothelin-degrading enzyme I; PreP, presequence peptidase.

Introduction

Neprilysin (NEP, EC 3.4.24.11) is a transmembrane M13 zinc metalloprotease that exhibits endopeptidase activity on over 30 short peptide substrates [1,2]. Recently, NEP has received considerable attention for its role in amyloid-β degradation and represents a potential therapeutic target in Alzheimer's disease research [3]. The enzyme is, however, better characterised for its role in blood pressure regulation through the degradation of several small peptide vasodilators which include bradykinin, substance P and natriuretic peptides [4].

The mechanism of degradation of three main classes of natriuretic peptides- atrial, B-type and C-type natriuretic peptides (ANP, BNP and CNP) by NEP are well documented [5]. These three classes of peptides have been studied for their promotion of vasodilation mediated through interaction with membrane guanylate cyclases and natriuretic receptors [6]. Whilst each peptide varies in length (between 22-32 amino acids), all share a common 17-residue central ring structure with 10 of the 17 residues conserved [6]. Differences in amino acid sequence causes varied susceptibility to NEP degradation as follows - CNP>ANP>BNP [7]. Their degradation and inactivation by NEP results in vasoconstriction and elevated blood pressure. As such, NEP has been targeted for inhibition in order to elicit an antihypertensive response in patients with high blood pressure [8].

The molecular structure of NEP is comprised of a 27-residue intracellular domain, followed by a 23-residue transmembrane domain and finally a 699-residue extracellular catalytic domain. To date, several crystal structures of the NEP extracellular domain have been reported for both substrate-free [9] and inhibitor-bound forms [10–15]. These structures reveal the domain is ellipsoid in shape with the active site contained within a large occluded cavity. The active site is based around the conserved metalloprotease HEXXH motif where two conserved histidine residues (His583 and His587) coordinate a zinc ion and the conserved glutamate (Glu584) is responsible for polarisation of a solvent molecule which then performs nucleophilic attack on the substrate's scissile peptide bond [16].

It should be noted that NEP and a few other zinc metalloproteases - including endothelin-converting enzyme I (ECE-1) [17], insulin degrading enzyme (IDE) [18], and presequence peptidase (PreP) [19] - are classed as cryptidases due to the location of the active site within a large cavity [20]. Each cryptidase must undergo a conformational change in which the structure transitions from open, where substrates can access the cavity, to closed where substrates are trapped, and substrate recognition can occur [20]. Cryptidases range in size from 85-120kDa and can degrade a many peptide substrate that vary in sequence, size, shape and surface charge.

The promiscuous nature of NEP, and other cryptidases, raises questions as to their mechanism of substrate specificity. NEP inhibitor-bound crystal structures have provided some insights into substrate specificity enabling the characterisation of S1, S1' and S2' [21] binding pockets at the catalytic site. S1' has been reported to be the largest contributor to substrate specificity having preference for hydrophobic amino acids. Specificity is also achieved through the limited cavity volume imposing constraints on maximal substrate size. For NEP the cavity volume of approximately 5000Å^3 results in selection of peptides under 5 kDa in size [22].

Despite the number of available NEP crystal structures, a peptide-bound complex has yet to be reported. This can be mainly attributed to rapid cleavage of peptides by NEP, hence not ideal for X-ray crystallography studies investigating protein-substrate binding interactions. Moreover, crystal growth, and subsequent data collection, of protein crystals requires lengthy periods of incubation, NEP would process any peptide substrate long before data collection could take place. In this study, a mutant NEP E584D protein was expressed and confirmed to be catalytically inactive. This protein was

used in the crystallographic study to prevent peptide cleavage and allow binding interactions to be preserved.

Here we report the structures of catalytically inactive NEP E584D in a substrate-free and peptide-bound form. In the peptide-bound form, a C-type natriuretic peptide (CNP) is bound to the active site, revealing main-chain binding interactions and providing insights into the general mechanism of peptide interaction. These results contribute to the understanding of a key enzyme NEP that has a role to play in both Alzheimer's disease and cardiovascular disease.

Materials and Methods

All reagents used were purchased from Sigma-Aldrich or Fisher Scientific unless otherwise specified.

Plasmid construction and transfection

cDNA encoding full length human NEP in cloning vector pMD18-T Simple was purchased from Sinobiology. Polymerase chain reaction (PCR) was used to, amplify the extracellular domain of NEP (Thr49 - Trp749), add a 5' KpnI site and 6x histidine tag, and add a 3' NotI site. The amplified PCR product and vector pPICzαA were digested with KpnI and NotI (NEB). The PCR product was then ligated into pPICzαA downstream of a secretion tag. This tag was transcribed with NEP for secreted protein expression but was cleaved after secretion.

Mutation of the NEP residue 584 from glutamate to aspartate (E584D) was conducted using PCR site-directed mutagenesis (NEB Q5) and confirmed using DNA sequencing. The NEP pPICzαA construct was integrated into the genome of *Pichia pastoris* GS115 in accordance with the Invitrogen EasySelect manual (cat. no. K1740-01) and restriction enzyme SacI (NEB). A full list of primer sequences are given in Table 1.

Protein expression and purification

Expression of recombinant NEP and NEP E584D extracellular domains from the *Pichia pastoris* GS115 was performed in accordance with the Invitrogen EasySelect manual. Briefly, a pre-induction culture was incubated for 24 hours in Buffered Glycerol-complex Medium (BMGY) to generate the desired cell density. Media was changed to Buffered Methanol-complex Medium (BMMY) for a 72-hour induction. 100% methanol was added at 24 and 48 hours to maintain the methanol concentration.

After induction the supernatant was harvested by centrifugation at 6000 RCF for 20 min at 4°C. Trizma and NaCl was added to the supernatant to give final concentrations of 25 mM Trizma and 150 mM NaCl. The supernatant was then centrifuged at 6000 RCF for 20 min at 4°C and filtered through a 0.22µm filter (Millipore).

Supernatant was loaded onto a 5 mL HisTrap affinity column (GE Healthcare Life Sciences) at 5 mL min^{-1} pre-equilibrated with Buffer A (25 mM Trizma, 150 mM NaCl and 2 mM $MgCl_2$ pH 7.5). After loading the column was washed with 2% Buffer B (25 mM Trizma, 150 mM NaCl, 2 mM $MgCl_2$ and 500 mM imidazole pH 7.5) until the UV trace returned to baseline. NEP was eluted using a single 50% Buffer B wash. Protein containing fractions were pooled and concentrated into 1 mL using a 30 kDa Millipore centrifuge filter. The concentrated NEP was loaded onto a 16/60 Superdex HiLoad 200 column for size exclusion. Again, protein containing fractions were pooled and stored at 4 °C for short term storage or −20 °C for longer term storage. SDS-PAGE was used to confirm presence and purity of NEP after purification.

Enzyme assay

The activity of NEP and NEP E584D were assessed by measuring cleavage of the fluorogenic peptide Mca-RPPGFSAFK-(Dnp) (Enzo Life Sciences) [23]. Protein was diluted to a concentration of 31.3nM in Buffer A. 50 µL of diluted protein was added to a black 96 well microplate (cat. no. 655076, Greiner Bio-One). 50 µL of 100 µM Mca-RPPGFSAFK-(Dnp), dissolved in Buffer A with 10% DMSO, was added to a black 96 well microplate (Greiner Bio-One) to initiate the reaction.

Each fluorescence assay was conducted in triplicate. Fluorescence was recorded at 20 second intervals for a length of 35 minutes on a CLARIOstar high-performance microplate reader (BMG LABTECK). Excitation was achieved at 328 nm and emission was detected at 393 nm [9].

Circular dichroism

The secondary structure composition of NEP and NEP E584D was analysed using circular dichroism. Protein samples of NEP and NEP E584D were diluted to 2.725 µM and 2.6 µM respectively before analysis. Data were collected in triplicate using a 1 mm quartz cuvette and a Chirascan circular dichroism spectrometer at 20ºC. The wavelength scanning range was between 200-300 nm with a 1 nm step size, monochromator bandwidth of 3 nm and sample time-per-point of 3 seconds.

Crystallisation

Protein crystallisation was performed using sitting drop vapour diffusion. NEP E584D (8 mg/mL) was dispensed with a Phoenix crystallisation robot (Art Robbins Instruments) into an Intelli-Plate 96 (cat. no. 102-0001-03, Art Robbins Instruments) at a ratio of 0.2 µL: 0.2 µL protein to crystallisation buffer. Crystallisation buffer for the substrate-free structure was 0.16 M potassium nitrate, 0.04M sodium bromide, 0.02 M bis-tris propane and 20% (w/v) PEG 3350. Crystallisation plates were incubated at 18 °C and crystals formed within two months.

Attempts to co-crystallize NEP E584D with peptide were unsuccessful. Instead the peptide-bound structure was achieved through soaking. Crystals for soaking were generated using crystallisation buffer 0.16 M potassium nitrate, 0.04 M sodium iodide and 20% (w/v) PEG 3350. Again, crystallisation plates were incubated at 18 °C and crystals formed within two months. Once formed 0.2 µl of 9.1 mM C-type natriuretic peptide was added to the crystallisation drops and incubated for a further 14 days at 18 °C before data collection. The C-type natriuretic peptide used had the amino acid sequence 'GLSKGCFGLKLDRIGSMSGLGC' and was sourced from GenScript (Cas. No. 127869-51-6). All crystals used for data collection were flash-cooled in liquid nitrogen for storage without the use of cryoprotectant.

X-ray data collection and refinement

X-ray diffraction data collection for the NEP E584D substrate-free and peptide-bound structures was conducted on Diamond Light Source (Didcot, Oxford UK) beamlines I04 (mx17212-37) and I04 (mx17212-46) respectively. At the time of collection both beam lines were fitted with Eiger2 X 16M detectors.

X-ray diffraction data were indexed and integrated using DIALS [24]. Data were scaled and merged using AIMLESS [25,26] where resolution cut offs were applied. The structures were solved by molecular replacement using Phaser [27] and substrate-free neprilysin (6GID) [9]. Programs Refmac5 [28] and Coot [29] were used for refinement of the structures.

Validation of the structures was achieved using programs MolProbity [30] and PDB validation [31]. All structural images and superpositions were generated in CCP4mg [32]. Final refined structures were deposited in the PDB under codes 6SH1 and 6SH2.

Results and Discussion

Catalytic inactivation of NEP

To investigate peptide binding interactions, it was necessary use catalytically inactive NEP. Inactive NEP could not perform peptide cleavage and hence allowed protein-peptide interactions to be preserved in crystallisation experiments. Similar crystallographic approaches have successfully been reported in the study of protein-peptide binding interactions with other catalytically inactive zinc metalloproteases [18,33].

Catalytic inactivation of NEP was achieved by mutation of active site glutamate 584 to an aspartate (E584D). DNA sequencing, as described in materials and methods, was used to confirm the presence of this mutation. The extracellular domain of NEP E584D was then expressed in *Pichia pastoris*. In the following results section, the extracellular domain of NEP E584D will be referred to as just NEP E584D. Activity of NEP E584D was measured using a fluorescence assay (Fig. 1). Unlike wild-type NEP, NEP E584D showed loss of catalytic activity. While no activity for NEP E584D was observed over the 35-minute assay there remained the possibility that low-level residual activity may still be present.

Circular dichroism (CD) was used to compare the secondary structure composition of NEP and NEP E584D. The high degree of similarity in CD traces confirmed that mutation E584D did not induce secondary structure variation (Fig. 2). As such, NEP E584D protein was considered suitable for crystallisation experiments.

Comparisons of NEP E584D and wild-type NEP substrate-free crystal structures

X-ray crystallography data for substrate-free NEP E584D were collected and the crystal structure (6SH1) was determined in the monoclinic space group $P2_1$ to a resolution of 2.1 Å. It should be noted that several lower resolution X-ray crystallography data sets for substrate-free NEP E584D were collected and solved in the more frequently observed $P3_221$ space group. Details of data collection and refinement statistics are listed in Table 2. The substrate-free structure of NEP E584D was used to determine whether the presence of mutation E584D caused significant structural perturbation from wild-type NEP.

Previously, we had reported the structure of wild-type substrate-free NEP (6GID) [9] to a resolution of 1.9 Å. This wild-type structure adopted a closed conformation and revealed the position of active site residues in a substrate-free state. Wild-type substrate-free NEP (6GID) was superimposed onto substrate-free NEP E584D (Fig. 3a). A root-mean-square deviation (RMSD) value of 0.57 Å, calculated using a least squares comparison for α-carbon residues 54–749, confirmed the overall structure had been preserved. The high degree structural similarity also confirmed that variation in space group between $P3_221$ and $P2_1$ did not cause structure changes due to crystal packing. NEP E584D remained in a closed conformation and contained the same four glycosylation sites. Electron density for the zinc ion remained clear and only minimal movement was present in residues surrounding or involved in zinc coordination (Fig. 3b). The only notable difference between wild-type and E584D substrate-free NEP structure was the molecule that provided additional coordination to the zinc ion. In wild-type substrate-free NEP a phosphate ion coordinates the zinc ion while in substrate-free NEP E584D a single water coordinates the zinc ion. The similarities between wild-type and mutant structures supported the view that NEP E584D was an appropriate model to study peptide binding interactions. Fourier electron density maps of residue 584 in NEP and NEP E584D highlight the presence of the mutation (Fig. 3c).

Peptide-bound crystal structure of NEP E584D

The peptide-bound crystal structure of NEP E584D (6SH2) was determined in the trigonal space group $P3_221$ to a resolution of 2.6 Å. The active site of NEP E584D, contained within the large central cavity, had sufficient electron density to model a four-residue peptide product from the 22-residue long C-type natriuretic peptide (CNP) (Fig. 4). These modelled residues occupied the S1, S1', S2' and S3' subsites that previously characterised in inhibitor-bound structures [10–15].

Previous high-performance liquid chromatography data for CNP has reported at least 6 cleavage sites are targeted by NEP [34]. The ability of NEP to cleave CNP at several distinct positions dictates that in a single protein crystal the residues of CNP interacting with the active site will be different in individual NEP molecules. Therefore, from the experimental X-ray crystallography data, whilst we were able to ascertain the mode of peptide binding for the α-carbon main-chain, we could not model the specific side-chains that occupy the S1-S3' subsites. Perhaps with higher resolution data it may be possible to identify the most common residues occupying these subsites in the conditions tested.

For the best interpretation of the electron density for CNP and to provide information on the mode of peptide binding, a poly-alanine tetra-peptide was modelled bound in the NEP E584D active site (Fig. 5a). A Fo-Fc Fourier difference map showed some continuation of electron density in areas of unmodelled side chains. Additional density was observed at the N- and C- terminus of the modelled peptide chain indicating the presence of additional residues that could not be resolved. The majority of CNP could not be modelled, suggesting much of the peptide is flexible (disordered) and does not exhibit tight binding interactions with the cavity lining. This also indicates that the modelled P1, P1', P2' and P3' residues are likely to be the primary site of interaction between NEP E584D and the peptide. An alternative possibility is that peptide cleavage had occurred due to low level protease activity undetected while performing enzyme assay measurements. However, the observed electron density between P1 and P1' was continuous indicating that no cleavage had occurred in the peptide fragment that was modelled.

Despite the inability to model the side chains of CNP, several binding interactions could be identified between the modelled poly-alanine main chain of CNP and NEP E584D (Fig. 5b). Based on our interpretation of the electron density we suggest that Asn542 and Ala543 interact with the amino group of P1'. Asn542 also interacts with the carboxyl group of P2'. Arg717 interacts with the carboxyl group of P1' and additional interactions are provided through coordination of the zinc ion by the carboxyl group of the P1 residue. Interestingly, these main chain interactions induce a >90º bend in the CNP around the P1' residue and their importance has been highlighted in previous inhibitor-bound structures. Phosphoramidon, a generic metallo-endopeptidase inhibitor, exhibits very similar binding interactions to the zinc ion, Asn542, Ala543 and Arg717 (Fig. 6a) [10]. This is also true of sacubitril, a NEP specific inhibitor, where all interactions except those from Ala543 are observed [15].

Further, residues Asn542, Ala543 and Arg717 are conserved in other metalloproteases including the previously mentioned cryptidases IDE, PreP and ECE-1. Peptide-bound structures for both IDE (2G47) and PreP (2FGE) reveal identical binding interactions to these conserved residues, leading to a highly similar peptide orientation. A superposition of peptide-bound NEP E584D and IDE structures (2G47) illustrates this observation (Fig. 6b). The high degree of similarity in peptide binding further validates our peptide-bound NEP E584D structure. In the absence of a peptide-bound structure of ECE-1, we predict a similar mode of peptide binding given the high structural homology to NEP.

In addition to the main chain interactions discussed above, peptide binding will also involve side-chain interactions. Whilst the side chains for CNP P1-P3' residues have not been modelled, the position of modelled β-carbons allows prediction of subsite residues that are important for protein-peptide

interactions (Figs. 5 and 7). The β-carbons for P1' and P2' are orientated towards NEP E584D residues therefore side chains are likely to have important roles in peptide binding. In contrast, P1 and P3' side chains are orientated into the cavity centre and are therefore unlikely to have close interactions with S1 and S3' sites.

The S1' and S2' sites have been characterised in inhibitor-bound structures [10–15] and exhibit several binding interactions. The S1' site is a hydrophobic pocket resulting in the reported preference of NEP to cleave substrates at the amino side of hydrophobic residues. S2' has been reported to have a preference for hydrophobic residues and can accommodate bulky side chains due to the movement involving residues Arg110, Arg102 and Phe106 [35,36].

Putative exosite

Additional unexplained electron density was observed in a proximal site approximately 14 Å away from the zinc ion in the peptide-bound NEP E584D structure (Fig. 8a). This density was completely absent in the substrate-free NEP E584D structure. It is likely that this density corresponds to a portion of CNP interacting with residues of the NEP E584D cavity. These interactions may anchor the peptide and explain why electron density is observed in this specific area. Whilst the exact region of CNP cannot be identified from electron density, the shape and size of the density can be accounted for by an amino acid residue (Fig. 8b). The modelled residue is orientated such that the electron density continues beyond the carboxyl and amino groups and the β-carbon is positioned towards polar residues Asp208, His217 and Tyr346 possibly indicating a preference for a polar residue in that location.

Similar electron density feature has been observed and reported in a peptide-bound structure of insulin-degrading enzyme (IDE) [18]. IDE, like NEP, is a zinc metalloprotease that degrades several small peptide substrates and possesses a catalytic site that is located within a large central cavity. In the peptide-bound structure of IDE, electron density was observed for residues around the catalytic zinc in addition to the proximal site. This proximal or exosite in IDE has been proposed to be important for positioning the peptide such that the correct residues are localised to the active site.

Whilst the peptide-bound structure reported here provides a strong indication for the presence of an exosite, complete certainty in the orientation of the interacting amino acid residue is lacking. Therefore, the peptide-bound structure has been submitted without this residue modelled. It is likely that higher resolution X-ray crystallography data may provide clarity to the existence of an exosite.

Conclusions

In summary, determination of a peptide-bound NEP E584D has revealed key binding interactions between protein and CNP. The main chain interactions observed for the P1-P3' residues are likely to be shared for all other NEP substrates.

Given that NEP peptide cleavage can occur at many locations where residue identity is varied, we conclude that peptide binding interactions between the main chain of P1-P3' and NEP E584D residues Asn542, Ala543 and Arg717 are most crucial for binding. These important interactions are conserved in cryptidases ECE-1, IDE and PreP. Additional interactions provided by the side chains of P1' and P2' residues will contribute to substrate selectivity but may not be as essential to binding.

Peptide residues not localised to the active site are likely to exhibit a high degree of flexibility within the central cavity, explaining the inability to identify them in this crystal structure. There was however an area of strong electron density observed in a site proximal to the active site. Similar density in a crystal structure of IDE has been reported as an exosite. While not fully clear, such sites might prove

to be critical for peptide binding by conferring the correct positioning of residues within the active site for cleavage. Further higher-resolution crystal structures may allow larger portions of the peptide to be resolved thereby providing additional information on peptide binding.

Acknowledgements
We thank Diamond Light Source for access to beamline I04 (proposal mx17212) that resulted in the data presented here. S.M. is supported by a post-graduate studentship from the Alzheimer's Society (UK) awarded to K.R.A. and V.S. [grant number – 286 (AS-PhD2015b-006)].

Author contributions
S.M. performed all the experiments, analysed the data and wrote the manuscript. V.S. supervised the study and edited the manuscript. K.R.A. conceptualised and supervised the study, analysed the data and edited the manuscript.

Additional information
Accession code: The atomic coordinates and structure factors (codes 6SH1 and 6SH2) have been deposited in the Protein Data Bank (http://www.pdb.org).

Competing financial interests
The authors declare no competing financial interests.

References

1 Erdös EG & Skidgel RA (1989) Neutral endopeptidase 24.11 (enkephalinase) and related regulators of peptide hormones. *FASEB J.* **3**, 145–151.

2 Rawlings ND, Barrett AJ, Thomas PD, Huang X, Bateman A & Finn RD (2018) The MEROPS database of proteolytic enzymes, their substrates and inhibitors in 2017 and a comparison with peptidases in the PANTHER database. *Nucleic Acids Res.* **46**, D624–D632.

3 Iwata N, Tsubuki S, Takaki Y, Shirotani K, Lu B, Gerard NP, Gerard C, Hama E, Lee HJ & Saido TC (2001) Metabolic regulation of brain Aβ by neprilysin. *Science.* **292**, 1550–1552.

4 Bayes-Genis A, Barallat J & Richards AM (2016) A test in context: neprilysin: function, inhibition, and biomarker. *J. Am. Coll. Cardiol.* **68**, 639–653.

5 Von Lueder TG, Sangaralingham SJ, Wang BH, Kompa AR, Atar D, Burnett JC & Krum H (2013) Renin–Angiotensin blockade combined with natriuretic peptide system augmentation. *Circ. Hear. Fail.* **6**, 594–605.

6 Korostyshevskaya IM, Maksimov VF & Rudenko NS (2016) C-Type natriuretic peptide: what, where and why? *Neurosci. Behav. Physiol.* **46**, 888–894.

7 Kenny AJ, Bourne A & Ingram J (1993) Hydrolysis of human and pig brain natriuretic peptides, urodilatin, C-type natriuretic peptide and some C-receptor ligands by endopeptidase-24.11. *Biochem. J.* **291**, 83–88.

8 Xu J, Carretero OA, Liu Y-H, Yang F, Shesely EG, Oja-Tebbe N & Yang X-P (2004) Dual inhibition of ACE and NEP provides greater cardioprotection in mice with heart failure. *J. Card. Fail.* **10**, 83–89.

9 Moss S, Subramanian V & Acharya KR (2018) High resolution crystal structure of substrate-free human neprilysin. *J. Struct. Biol.* **204**, 19–25.

10 Oefner C, D'Arcy A, Hennig M, Winkler FK & Dale GE (2000) Structure of human neutral endopeptidase (neprilysin) complexed with phosphoramidon. *J. Mol. Biol.* **296**, 341–349.

11 Oefner C, Roques BP, Fournie-Zaluski M-C & Dale GE (2004) Structural analysis of neprilysin with various specific and potent inhibitors. *Acta Crystallogr. Sect. D Biol. Crystallogr* **60**, 392–396.

12 Sahli S, Frank B, Schweizer WB, Diederich F, Blum-Kaelin D, Aebi JD, Böhm H, Oefner C & Dale GE (2005) Second-generation inhibitors for the metalloprotease neprilysin based on bicyclic heteroaromatic scaffolds: synthesis, biological activity, and X-ray crystal-structure analysis. *Helv. Chim. Acta* **88**, 731–750.

13 Oefner C, Pierau S, Schulz H & Dale GE (2007) Structural studies of a bifunctional inhibitor of neprilysin and DPP-IV. *Acta Crystallogr. Sect. D Biol. Crystallogr* **63**, 975–981.

14 Glossop MS, Bazin RJ, Dack KN, Fox DNA, MacDonald GA, Mills M, Owen DR, Phillips C, Reeves KA, Ringer TJ, Strang RS & Watson CAL (2011) Synthesis and evaluation of heteroarylalanine diacids as potent and selective neutral endopeptidase inhibitors. *Bioorg. Med. Chem. Lett.* **21**, 3404–3406.

15 Schiering N, D 'arcy A, Villard F, Ramage P, Logel C, Cumin F, Ksander GM, Wiesmann C, Karki RG & Mogi M (2016) Structure of neprilysin in complex with the active metabolite of sacubitril. **6**, 27909.

16 Gomis-Rüth F (2008) Structure and mechanism of metallocarboxypeptidases. *Crit. Rev. Biochem. Mol. Biol.* **43**, 319–345.

17 Schulz H, Dale GE, Karimi-Nejad Y & Oefner C (2009) Structure of human endothelin-converting enzyme I complexed with phosphoramidon. *J. Mol. Biol.* **385**, 178–187.

18 Shen Y, Joachimiak A, Rosner MR & Tang W-J (2006) Structures of human insulin-degrading enzyme reveal a new substrate recognition mechanism. *Nature* **443**, 870–874.

19 Johnson KA, Bhushan S, Ståhl A, Hallberg BM, Frohn A, Glaser E & Eneqvist T (2006) The closed structure of presequence protease PreP forms a unique 10 000 $Å^3$ chamber for proteolysis. *EMBO J.* **25**, 1977–1986.

20 Malito E, Hulse RE & Tang W-J (2008) Amyloid-β degrading cryptidases: insulin degrading enzyme, presequence peptidase, and neprilysin. *Cell. Mol. Life Sci.* **65**, 2574–2585.

21 Schechter I & Berger A (1967) On the size of the active site in proteases. I. Papain. *Biochem. Biophys. Res. Commun.* **27**, 157–162.

22 Macours N, Poels J, Hens K, Francis C & Huybrechts R (2004) Structure, Evolutionary Conservation, and Functions of Angiotensin- and Endothelin-Converting Enzymes. In pp. 47–97.

23 Johnson GD & Ahn K (2000) Development of an internally quenched fluorescent substrate selective for endothelin-converting enzyme-1. *Anal. Biochem.* **286**, 112–118.

24 Waterman DG, Winter G, Gildea RJ, Parkhurst JM, Brewster AS, Sauter NK & Evans G (2016) Diffraction-geometry refinement in the DIALS framework. *Acta Crystallogr. Sect. D Biol. Crystallogr.* **39**, 558–575.

25 Evans PR & Murshudov GN (2013) How good are my data and what is the resolution? *Acta Crystallogr. Sect. D Biol. Crystallogr.* **69**, 1204–1214.

26 Winn MD, Ballard CC, Cowtan KD, Dodson EJ, Emsley P, Evans PR, Keegan RM, Krissinel EB, Leslie AGW, McCoy A, McNicholas SJ, Murshudov GN, Pannu NS, Potterton EA, Powell HR, Read RJ, Vagin A, Wilson KS & IUCr (2011) Overview of the CCP4 suite and current developments. *Acta Crystallogr. Sect. D Biol. Crystallogr.* **67**, 235–242.

27 McCoy AJ, Grosse-Kunstleve RW, Adams PD, Winn MD, Storoni LC & Read RJ (2007) Phaser crystallographic software. *J. Appl. Crystallogr.* **40**, 658–674.

28 Murshudov GN, Skubák P, Lebedev AA, Pannu NS, Steiner RA, Nicholls RA, Winn MD, Long F & Vagin AA (2011) REFMAC5 for the refinement of macromolecular crystal structures. *Acta Crystallogr. Sect. D Biol. Crystallogr.* **67**, 355–367.

29 Emsley P, Lohkamp B, Scott WG & Cowtan K (2010) Features and development of Coot. *Acta Crystallogr. Sect. D Biol. Crystallogr.* **66**, 486–501.

30 Chen VB, Arendall WB, Headd JJ, Keedy DA, Immormino RM, Kapral GJ, Murray LW, Richardson JS & Richardson DC (2010) MolProbity: all-atom structure validation for macromolecular crystallography. *Acta Crystallogr. Sect. D Biol. Crystallogr.* **66**, 12–21.

31 Berman H, Henrick K & Nakamura H (2003) Announcing the worldwide Protein Data Bank. *Nat. Struct. Mol. Biol.* **10**, 980.

32 McNicholas S, Potterton E, Wilson KS & Noble MEM (2011) Presenting your structures: the CCP4mg molecular-graphics software. *Acta Crystallogr. Sect. D Biol. Crystallogr.* **67**, 386–394.

33 Teixeira PF, Masuyer G, Pinho CM, Branca RMM, Kmiec B, Wallin C, Wärmländer SKTS, Berntsson RP-A, Ankarcrona M, Gräslund A, Lehtiö J, Stenmark P & Glaser E (2018) Mechanism of peptide binding and cleavage by the human mitochondrial peptidase neurolysin. *J. Mol. Biol.* **430**, 348–362.

34 Watanabe Y, Nakajima K, Shimamori Y & Fujimoto Y (1997) Comparison of the hydrolysis of the three types of natriuretic peptides by human kidney neutral endopeptidase 24.11. *Biochem. Mol. Med.* **61**, 47–51.

35 Howell S, Nalbantoglu J & Crine P (1995) Neutral endopeptidase can hydrolyze β-amyloid(1–40) but shows no effect on β-amyloid precursor protein metabolism. *Peptides* **16**, 647–652.

36 Sexton T, Hitchcook LJ, Rodgers DW, Bradley LH & Hersh LB (2012) Active site mutations change the cleavage specificity of neprilysin. *PLoS One* **7**, 1–10.

Figure legends

Figure 1. Enzymatic assay confirming NEP E584D inactivation. NEP or NEP E584D was incubated with reporter peptide Mca-RPPGFSAFK(Dnp). Cleavage of the reporter peptide produces detectable fluorescence which is recorded over time. Above, assays for Mca-RPPGFSAFK(Dnp) cleavage by NEP or NEP E584D are shown. The average of three assays has been plotted at each data point with standard error bars.

Figure 2. Circular dichroism comparison between wild-type NEP and NEP E584D. The overlapping traces confirm NEP E584D has the same secondary structure composition as wild-type NEP and are indicative of a largely α-helical protein.

Figure 3. Comparison of NEP and NEP E584D crystal structures. (a) a superposition of the substrate-free NEP (6GID) (pink) and NEP E584D (6SH1) (turquoise) crystal structures. (b) a stereo view of the superimposed active site residues. Electron density for residues E584 (6GID) and D584 (6SH1) (c). 2Fo-Fc maps are set to a contour level of 1σ.

Figure 4. Electrostatic surface representation of NEP E584D (6SH2) with bound CNP. The location of bound peptide (yellow) is shown with the catalytic zinc ion (orange).

Figure 5. CNP electron density and binding interactions. (a) the modelled peptide fragment is shown with localised 2Fo-Fc and Fo-Fc omit electron density maps (6SH2). 2Fo-Fc and Fo-Fc maps are set to contour levels of 1σ and 3σ respectively. (b) a stereo view of the modelled peptide fragment with surrounding active site residues. Close range interactions are marked with dashed lines.

Figure 6. Comparison of conserved active site residues and their role in substrate/inhibitor binding. Stereo views of peptide-bound NEP E584D (6SH2) (blue) superimposed onto (a) the Phosphoramidon-bound NEP structure (1DMT) (green) and (b) peptide-bound IDE structure (2G47) (green). The P1-P3' residues of the bound peptide in NEP E584D are shown in yellow. Phosphoramidon and IDE bound peptide are shown in magenta. Close range interactions between peptide and protein are marked with dashed lines.

Figure 7. Schematic of binding interactions between NEP E584D and P1, P1' and P2' residues of CNP.

Figure 8. Putative exosite electron density and nearby residues. (a) 2Fo-Fc and Fo-Fc omit electron density maps for the putative exosite with close NEP E584D amino acids (6SH2). 2Fo-Fc and Fo-Fc maps are set to contour levels of 1σ and 3σ respectively. (b) an alternative orientation of the exosite density with modelled alanine presented as a stereo view.

Table 1. Primer sequences used for NEP E584D clone creation.

Cloning in pPICzαA	**Primer sequence**
Forward	CGCTGGTACCCATCACCACCACCATCACGAATTCCGGACCTACGATGATGGTATTTGCAAG
Reverse	GCTTGCGGCCGCTCACCAAACCCGGCACTTC
Mutagenesis	
Forward	CATAGGACACCAAATCACCCATGGCTTCG
Reverse	ACCATGCCGATGCCCCCA

Table 2. NEP E584D X-ray crystallography and refinement statistics.

	Substrate-free	**Peptide-bound**
Beamline	I04, DLS	I03, DLS
Wavelength (Å)	0.9795	0.9762
Crystallographic statistics		
Space group	$P2_1$	$P3_221$
Unit cell dimensions		
a,b,c (Å)	76.14, 99.75, 100.12	109.27, 109.27, 112.58
α, β, γ (º)	90.00, 106.23, 90.00	90.00, 90.00, 120.00
Resolution range (Å)	69.22-2.10 (2.14-2.10)	72.44-2.60 (2.72-2.60)
R merge	0.178 (3.676)	0.144 (6.977)
$CC_{1/2}$	0.992 (0.464)	1.000 (0.604)
⟨I/σ (I)⟩	6.6 (1.0)	17.3 (1.0)
Completeness (%)	99.9 (99.8)	100 (100)
No. observed reflections	576297 (32234)	973293 (107982)
No. unique reflections	83834 (4581)	24386 (2945)
Multiplicity	6.9 (7.0)	39.9 (36.7)
Refinement statistics		
R_{work} /R_{free} (%)	21.94/26.35	24.43/28.82
R.m.s deviations		
Bond lengths (Å)	0.003	0.002
Bond angles (º)	1.212	1.148
Ramachandran statistics		
Favoured (%)	97	96
Allowed (%)	3	4
Outliers (%)	0	0
Wilson B-factor (Å²)	39.9	84.3
Average B-factors (Å²)		
Protein atoms	44.54	102.18
Ligand atoms	-	104.16
Water molecules	42.67	62.68
Zinc ion	34.10	81.62
No. of atoms		
Protein	11226	5512
Ligand	-	19
Water	495	1
Zinc ion	2	1
PDB code	**6SH1**	**6SH2**

Values in parentheses are for highest-resolution shell.

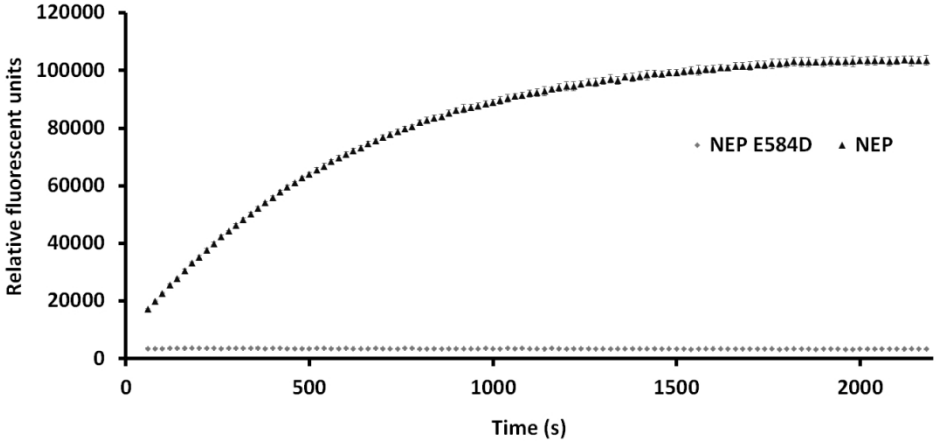
120000
100000
80000
60000
40000
20000
0
Relative fluorescent units
0
500
1000
1500
2000
Time (s)
NEP E584D
NEP

Figure 1

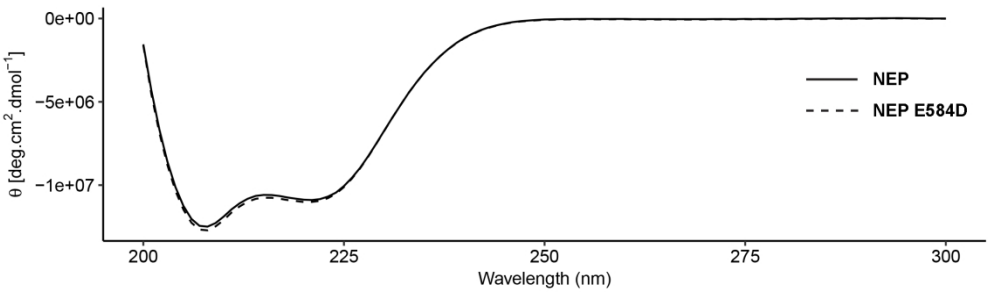
0e+00
−5e+06
−1e+07
θ [deg.cm^2.dmol^{-1}]
200
225
250
275
300
Wavelength (nm)
NEP
NEP E584D

Figure 2

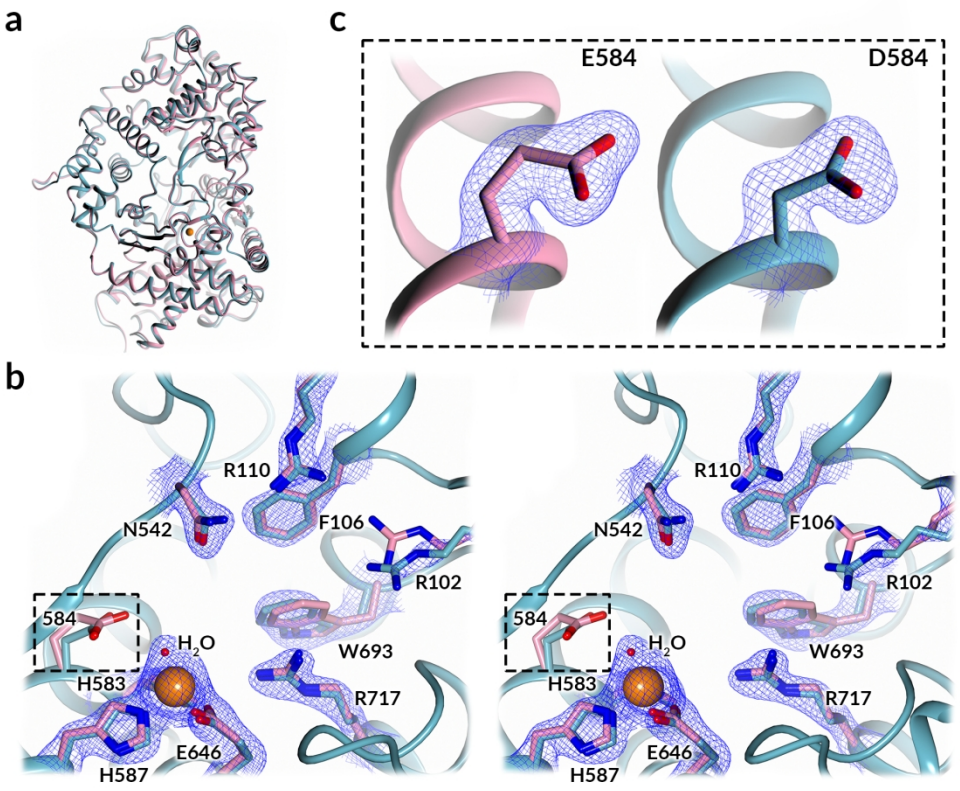

Figure 3

175x142mm (300 x 300 DPI)

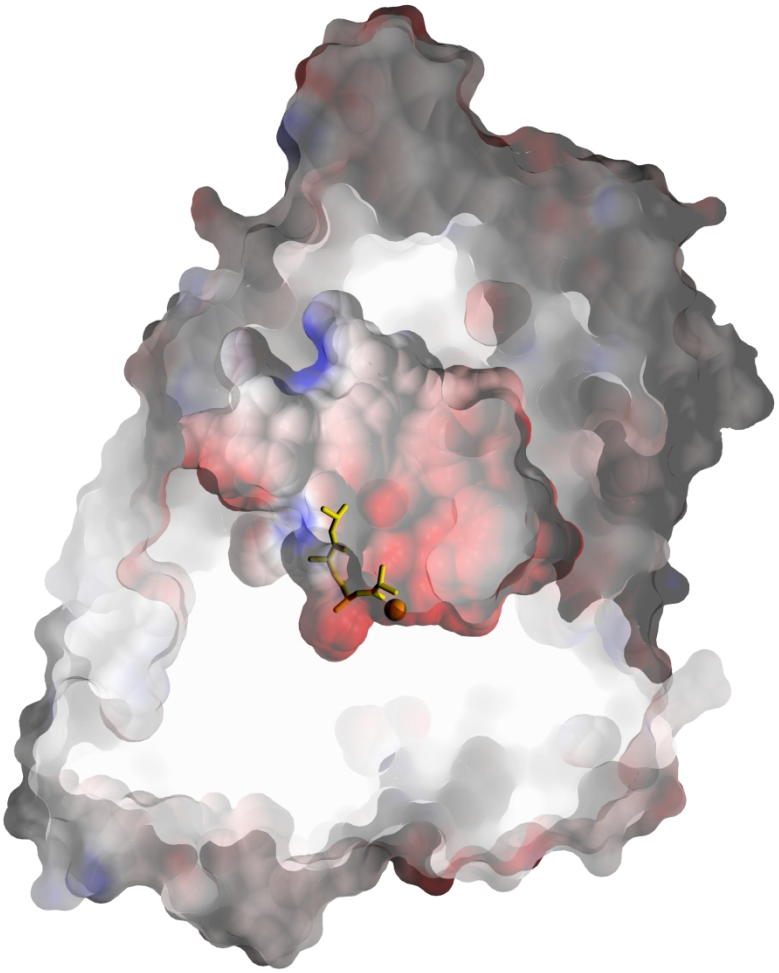

Figure 4

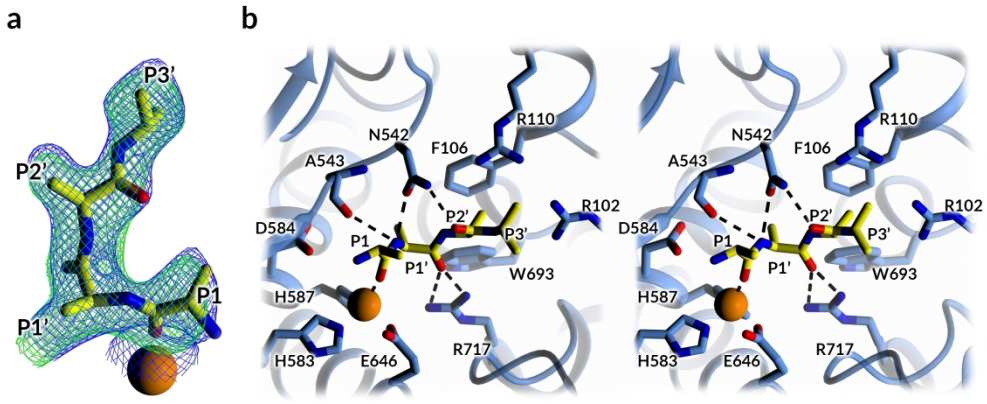
a
b
P3'
P2'
P1
P1'
N542
F106
R110
A543
R102
D584
P2'
P1
P3'
P1'
W693
H587
H583
E646
R717

Figure 5

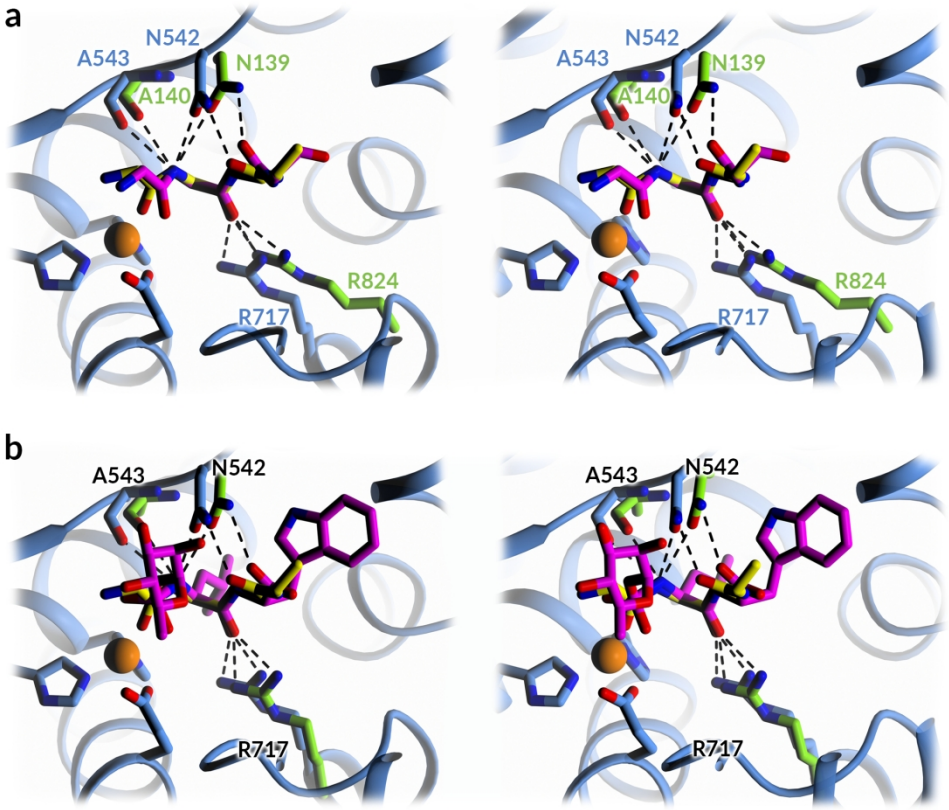
a
N542
A543
N139
A140
R824
R717
N542
A543
N139
A140
R824
R717
b
A543
N542
R717
A543
N542
R717

Figure 6

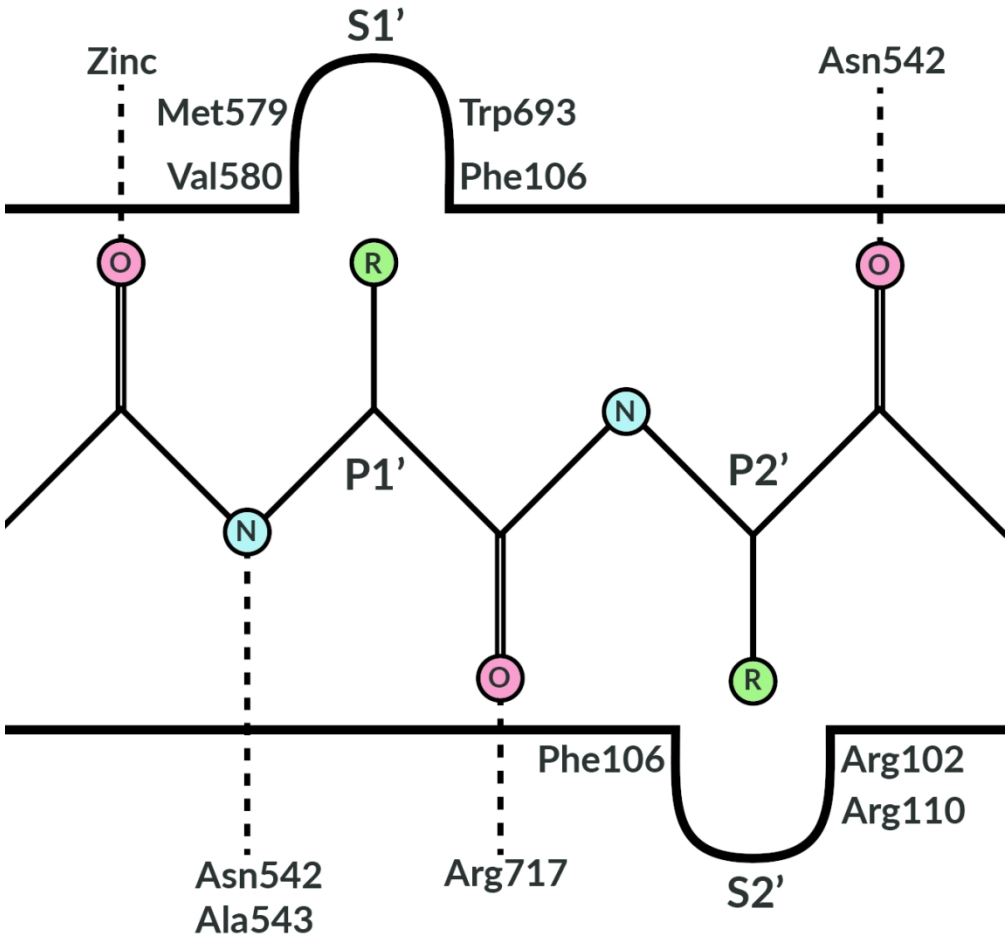
S1'
Zinc
Asn542
Met579
Trp693
Val580
Phe106
O
R
O
N
P1'
N
P2'
O
R
Phe106
Arg102
Arg110
Asn542
Ala543
Arg717
S2'

Figure 7

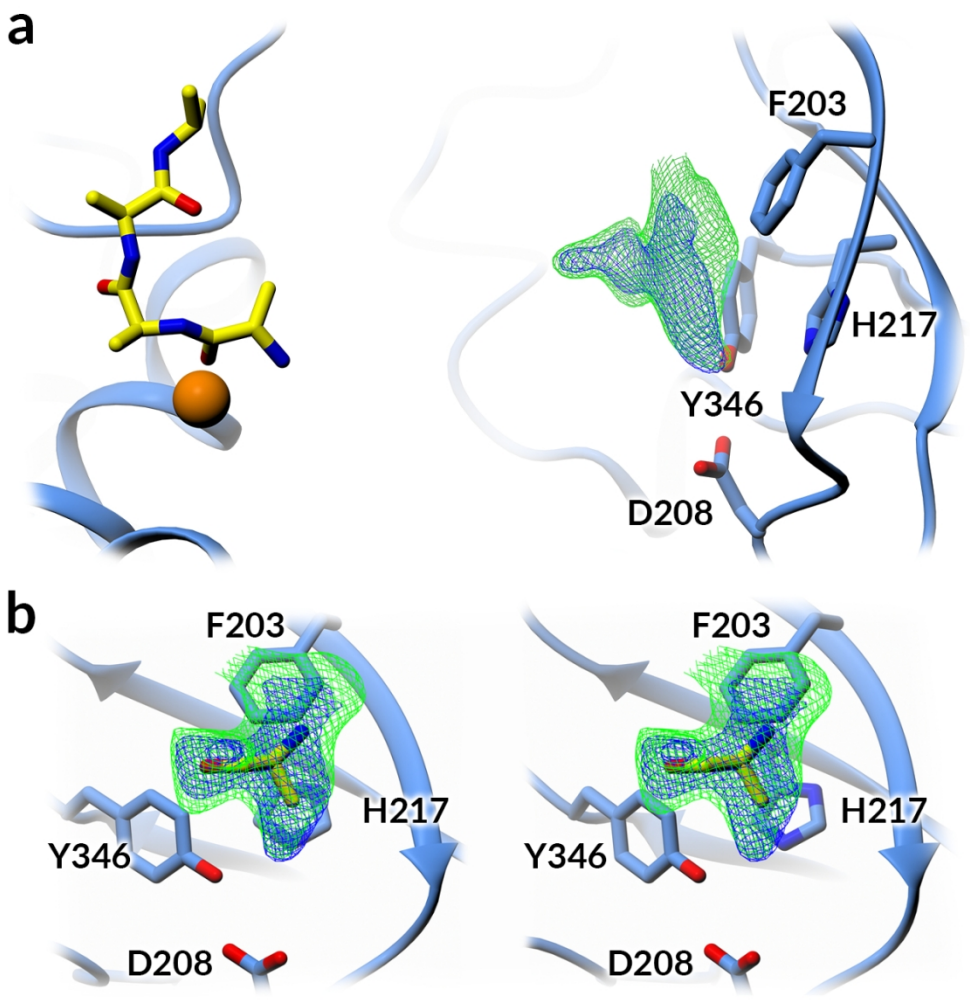
a
F203
H217
Y346
D208
b
F203
H217
Y346
D208
F203
H217
Y346
D208

Figure 8